Journal of Alloys and Compounds 649 (2015) 495–499

Contents lists available at ScienceDirect

Journal of Alloys and Compounds

journal homepage: http://www.elsevier.com/locate/jalcom

Letter

Effect of aging on interface characteristics of Al–Mg–Si/SiC composites

Keywords:
Metal matrix composite
Interfacial reaction
Age-hardening
Transmission electron microscopy

A B S T R A C T

The interface characteristics of Al–Mg–Si/SiC composites from the supersaturated to peak-aged time state are investigated mainly by electron microscopy including scanning transmission electron microscopy (STEM) and high-resolution transmission electron microscopy (HRTEM). The experimental results show that MgO is the main interfacial reaction product at the beginning of aging. At the peak-aged time, the content level of Mg in matrix is decreased due to the precipitation of Mg_2Si precipitate during aging, resulting in the formation of a $MgAl_2O_4$ phase which becomes the main reaction product at the SiC/Al interface, and these $MgAl_2O_4$ nanoparticles can improve the bonding strength of interface.

1. Introduction

Compared to the monolithic alloys, the addition of SiC reinforcement into Al–Mg–Si alloys can raise their performance limits. Aluminum Matrix Composites (AMCs) are designed to have the required toughness of the alloy matrix along with the desired hardness, stiffness and strength of hard ceramic reinforcements. AMCs can have widespread applications in various industries such as for aerospace, energy and military purposes [1,2].

The distribution of SiC particles in Al matrix will strongly affect the mechanical properties of AMCs. Hence, suitable parameters of mixing and secondary processing are chosen to improve the distribution of SiC particles in Al matrix [3]. Furthermore, the interfaces between the SiC reinforcement and the metal matrix in AMCs also play an important role in determining their mechanical properties. Usually, the possible interfacial reactions can be expressed as follows [4–7]:

$$2SiO_2 + 2Al + 5Mg = MgAl_2O_4 + 2Mg_2Si \quad (1)$$

$$4Mg + SiO_2 = 2MgO + Mg_2Si \quad (2)$$

$$4Al + 3SiO_2 = 2Al_2O_3 + Si \quad (3)$$

The purposes of Mg addition are manifold, because it can promote the formation of spinel ($MgAl_2O_4$) or MgO at the oxidized SiC/Al interface (Eqs. (1) and (2)), enhance the wetting behavior of the SiC particles with the matrix [8], and thus improve the interfacial bonding. It has been reported that the bonding strength between $MgAl_2O_4$ and Al is higher than that between Al_4C_3 and Al [9,10]. In this paper, the features of interface between SiC and metal matrix from the supersaturated to peak time state have been clarified by using electron microscopy including STEM elemental mapping with Super-X detector and HRTEM imaging with an image corrector.

2. Materials and experimental

The Al–Mg–Si/SiC composites were produced by powder metallurgy technique including high ball milling of inert gas atomized powders of Al 6066 (The chemical composition was Al–1.2 wt.% Mg–1.1 wt.%Si–0.9 wt.%Cu), commercial 2Mg vol.% and 3SiC vol.% with an average size of 100, 5–10 and 1–10 μm, respectively, followed by an extrusion at the ratio of 29.0 after soaking at 480 °C for 0.5 h. Then the samples were hot-rolled to the sheets of a 4 mm thickness at 480 °C. The hot-rolled sheets were solution treated at 520 °C for 2 h, and then quenched into water at room temperature. Subsequently, some sheets were aged at 180 °C for various times. Vickers hardness tests were carried out with an HV-10B machine using a weight of 5 kg, and the presented hardness values were the average of five tests. The tensile tests of all samples are carried out by a WDT-30 machine with an initial strain rate of $5 \times 10^{-4}\ s^{-1}$ in the long transverse direction, using 25 mm gauge length specimens.

XRD experiments were carried out on a Diffractometer Rigaku D/max 2550 to identify the phases. Scanning electron microscopy (SEM) examinations were carried out with a SIRION 200 SEM. The transmission electron microscopy (TEM) characterizations and STEM elemental mappings were conducted using a Titan G2 60-300 TEM with an image corrector and a Super-X detector, operating at 300 KV. The TEM samples were prepared by mechanically grinding, polishing, dimpling and finally ion-milling using a Gatan PIPS 691.

3. Results and discussion

Fig. 1a is a SEM image of the SiC powder, showing that the size of polyhedral SiC particles is in the range between 1 μm and 10 μm. Fig. 1b and c shows typical microstructures of the supersaturated

http://dx.doi.org/10.1016/j.jallcom.2015.07.033
0925-8388/

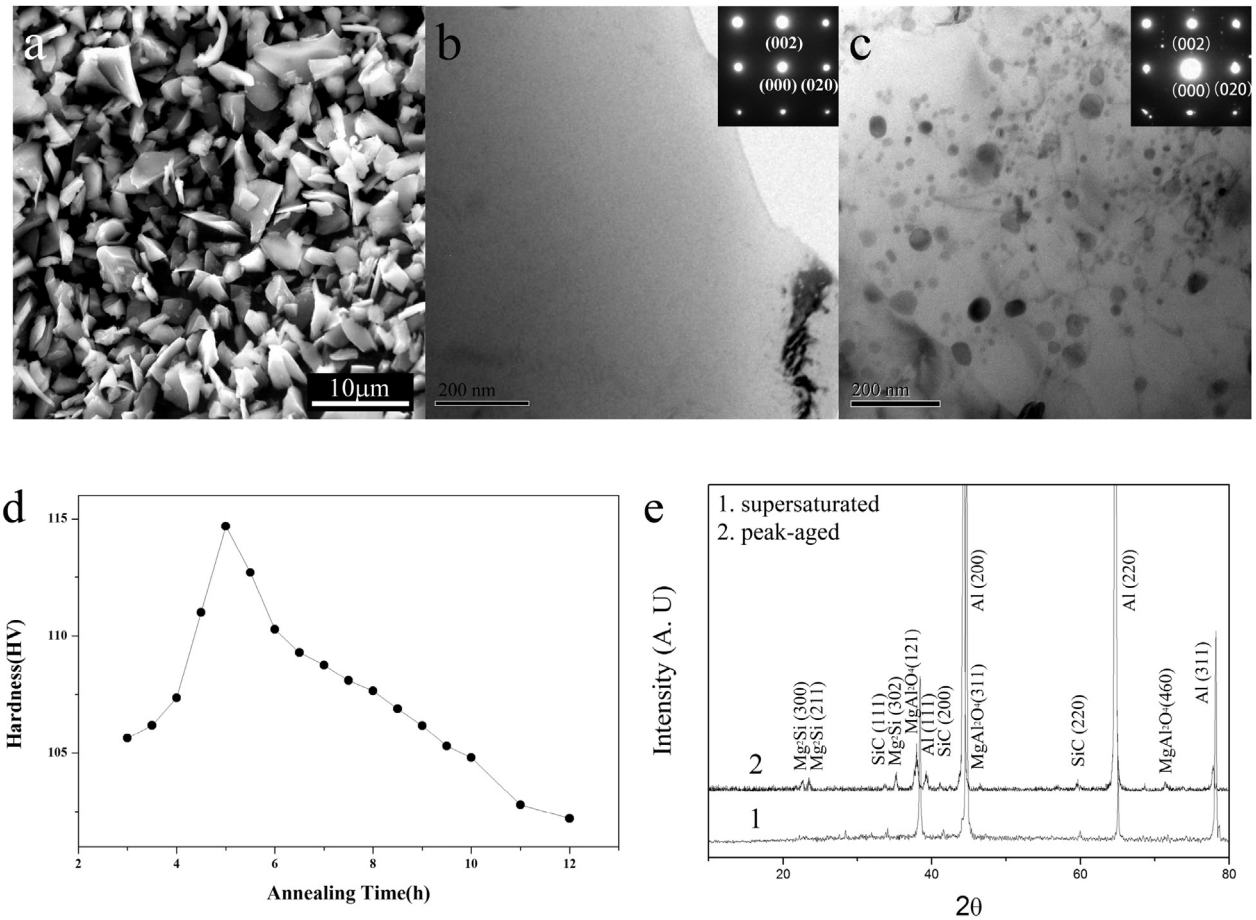

Fig. 1. (a) SEM image of the SiC particles, (b) TEM bright field (BF) image under the supersaturated condition, (c) TEM BF image under the peak-aged condition, (d) Hardness versus aging time curve for supersaturated 6066/3SiC/2Mg (vol.%) composite, (e) X-ray diffraction profiles of the supersaturated composite and peak-aged composite.

composites and the peak-aged samples, respectively, in which no precipitates can be seen in the saturated state while a distribution of Mg_2Si β precipitates can be observed in the peak-aged state, and a representative hardness-time curve of supersaturated composites after various aging times is given in Fig. 1d, which shows that in the aging processes, the value of hardness increases with the increase in aging time, reaches its maximum aging at a time of 5 h, and after 5 h, it decreases with increasing aging time. An exemplary XRD diffraction pattern is given in Fig. 1e, from which the diffraction peaks for both SiC and Al matrix can be observed for the supersaturated composites while Mg_2Si and $MgAl_2O_4$ phases can be observed for the peak-aged samples. On the features of SiC/Al interface in composites, our study is focused on the supersaturated state and the peak-aged state because they are most important ones for aging treatment.

In composites, the fracture mechanism of SiC particle, namely if it is a tensile loading-induced SiC particle fracture or a particle pull-out, is controlled by the relationship between SiC particle strength and SiC/Al interface strength. A particle pull-out fracture will be the predominant mode if the particle strength is higher, while a tensile loading-induced SiC particles fracture will be the predominant one if the interface strength is higher [11]. SEM images in Fig. 2 show the tensile fracture surface characteristics of the composites treated at two different conditions, from which the fracture dimples can be easily noticed on the fracture surface for both the conditions. Many particles also can be seen on the fracture surface, which are marked by white circles. EDX measurements were carried out on the particle "A" (Fig. 2a) and the particle "B" (Fig. 2c) in the composites at two different conditions, respectively. The EDX results are displayed in Fig. 2e, indicating that these particles are SiC. When the decohesion of SiC/Al interface occurs, an effective interfacial debonding between the matrix alloy and the SiC particle can be observed in Fig. 2a and b. Obvious cracks between the SiC particle and matrix can be clearly seen. In contrast, when a tensile loading-induced SiC particles fracture occurs, the cleavage planes of SiC particles in a ductile dimple still tightly surrounded by Al matrix are exposed on the SiC fracture surfaces (Fig. 2c and d), exhibiting a characteristic brittle fracture. Moreover, the fracture surface appearance of SiC particles in the peak-aged condition is quite flat, which is in a sharp contrast to the comparatively rough fracture surface of SiC particles in the supersaturated condition because some remaining matrix layers are often found to adhere to the SiC particle surface. For SiC particles, it is therefore mainly a particle pull-out fracture in the supersaturated composites while it is mainly a tensile loading-induced particle fracture in the peak-aged ones, which indicates a stronger bonding strength of SiC/Al interface under the peak-aged condition than the supersaturated condition.

Fig. 3 presents the angular dark field (ADF) STEM images and elemental mapping results showing the microstructural characteristics of typical SiC/Al interfaces of the supersaturated and peak-aged composites, respectively. The results reveal the typical change of interfacial reaction products in the composites at two different aging states. In Fig. 3a, a thin bright layer of a few nanometers